'92 KACC 1992. 10. 19~21

An Inverse Dynamic Trajectory Planning for the End-Point Tracking Control of a Flexible Manipulator*

Dong-Soo Kwon and Scott M. Babcock

Robotics & Process Systems Division
Oak Ridge National Laboratory
P.O. Box 2008
Oak Ridge, TN 37831-6304

Wayne J. Book

George W. Woodruff School of
Mechanical Engineering
Georgia Institute of Technology
Atlanta, GA 30332

ABSTRACT

A manipulator system that needs significantly large workspace volume and high payload capacity has greater link flexibility than typical industrial robots and teleoperators. If link flexibility is significant, position control of the manipulator's end-effector exhibits the nonminimum phase, noncollocated, and flexible structure system control problems. This paper addresses inverse dynamic trajectory planning issues of a flexible manipulator. The inverse dynamic equation of a flexible manipulator was solved in the time domain. By dividing the inverse system equation into the causal part and the anticausal part, the inverse dynamic method calculates the feedforward torque and the trajectories of all state variables that do not excite structural vibrations for a given end-point trajectory. Through simulation and experiment with a single-link flexible manipulator, the effectiveness of the inverse dynamic method has been demonstrated.

1. Introduction

A manipulation system such as the long-reach manipulator for nuclear waste remediation or the space shuttle arm, which requires large workspace volume and high payload capacity, has greater link flexibility than typical industrial robots and teleoperators. If link flexibility is significant, control of the end-effector's position will cope with the nonminimum phase, noncollocated, and flexible structure control problems. The flexible manipulator system should be able to follow a given end-point trajectory to be used as a practical robotic manipulator in spite of its flexibility. This paper proposes a simple time-domain inverse dynamic method that enables a flexible manipulator to follow a given end-point trajectory accurately without overshoot or residual vibration.

The feedback regulating control is one of the typical methods used to suppress the structural vibration of a manipulator. By using joint and strain feedback control, Hastings and Book [7] demonstrated structural vibration could be damped successfully. Even though the feedback control can dampen the structural vibration, their experiment showed undershoot, overshoot, and flexible vibration to a step response. For a step input command, these vibration phenomena are inevitable with the feedback control scheme because the feedback control signal contains high frequency components that excite natural frequencies of the system. Instead of a step command, a smooth nominal trajectory should be used as the joint reference command of tracking control. However, the desired trajectories of flexible mode variables are necessary to produce the desired output trajectories such as joint and strain. In the absence of desired flexible mode values, it has been acceptable to assign a zero value to each desired flexible mode values to suppress vibration. In other words, reference commands are given to the flexible manipulator to follow the trajectory like a rigid manipulator. Even though the feedback tracking control reduces the vibration, such unrealistic commands always generate vibration.

To avoid the above trajectory generation problem, De Luca and Siciliano [6] suggested a joint-based inversion control scheme. This method showed good tracking results for a certain joint trajectory, but it could not be extended to an end-point trajectory following control, because of nonminimum phase system characteristics. Oosting and Dickerson [8] proposed a calculation method of the torque to follow a smooth trajectory with the simple lumped-parameter model of a two-link flexible manipulator.

To make the end-point of a flexible manipulator follow a given trajectory, Bayo [2] proposed a new approach. For a given end-point acceleration profile, the required torque was calculated by solving the inverse dynamic equation in the frequency domain through the inverse fast Fourier transform. Bayo pointed out that the inverse dynamic system where the end-point acceleration is the input and the joint torque is the output is a noncausal system because the output (torque) must begin before the input (end-point acceleration) begins. In spite of the excellent results reported, this method has a drawback. It requires extensive computation for the transformation of the dynamic model and the input trajectory from the time domain to the frequency domain. It also requires the inverse transformation of the output back to the time domain. To reduce this computational burden, Bayo and Moulin [4] introduced the convolution integral method to solve the inverse dynamic equation.

Asada and Ma [1] derived an inverse dynamic equation by using assumed mode functions for a general n-link case. Since the transfer function of a flexible manipulator between the input (torque) and the output (end-point position) is a nonminimum phase system, it has some positive real value zeros. These zeros become positive poles of the inverse dynamic system transfer function. They cause the inverse

* Research sponsored by the Office of Technology Development, U.S. Department of Energy, under contract DE-AC05-84OR21400 with Martin Marietta Energy Systems, Inc., and by the National Aeronautics and Space Administration under Grant No. NAG 1-623.

system to be unstable if the inverse system output is restricted to causal solutions. Asada and Ma showed nonlinear effecfts using rigid motion torque without solving the inverse dynamic equation completely.

Kwon and Book [12] introduced a new inverse dynamic method that considerably relieves the calculation burden. The required torque was calculated in the time domain, and the desired trajectories of flexible mode coordinates were obtained to dynamically match the given end-point trajectory. These trajectories are used as reference commands of flexible coordinates for feedback tracking control. This trajectory generation considering flexible dynamics is the distinctive advantage of this time-domain inverse dynamic method.

This paper presents the inverse dynamic method with the detailed interpretation of this method in the frequency domain. First, a single-link manipulator is described and modeled by using the assumed mode method. Second, the time-domain inverse dynamic system equation is derived from the dynamic model in a state space form. Third, the time-domain inverse dynamic method is explained in the frequency domain. Next, this inverse dynamic method is implemented through simulations on the single-link flexible manipulator shown in Figure 1. Results are compared with the output of other typical control methods. Finally, a tracking controller was designed that combines the inverse dynamic feedforward control and the joint feedback control, and its experimental results are presented and discussed.

2. Modeling

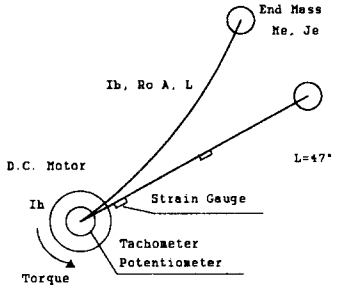

Figure 1. A single link flexible manipulator

A single-link flexible manipulator having planar motions is described as shown in Figure 1. The link is made of aluminum beam (3/16"x1"x47"), and it is modeled with the rotational inertia, Ib, and the unit length mass, RoA. The rotating inertia of the servo motor, the tachometer, and the clamping hub are modeled as the hub inertia, Ih. The payload is modeled as the end mass, Me, and the rotational inertia, Je. Though structural damping exists in the flexible link, it is ignored in modeling.

To derive equations of motion of the manipulator, we describe the position of a point on the beam with virtual rigid body motion and flexible deflection by using a Bernoulli-Euler beam model. The virtual rigid body motion is represented by the motion of the moving coordinate attached to the beam. The flexible deflection is described by a finite series of assumed modes with respect to that moving reference frame.

Defining the rigid body motion is important because different mode shape functions have to be used according to the choice of the rigid body coordinate. Several authors [7,9]

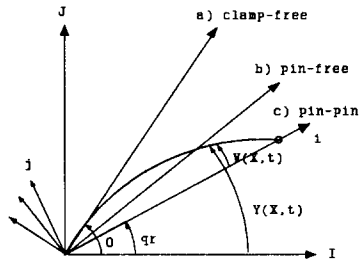

Figure 2. The kinematic descriptions of flexible manipulator coordinates

have used the rigid body coordinate that is attached at the base hub like (a) of Figure 2 with the clamp-free boundary condition mode functions. Other authors [5] defined the rigid body coordinate to pass through the center of mass of the beam and used pin-free mode functions, (b). Others [1] let the rigid body coordinate pass through the end-point and used the pin-pin mode functions, (c). All these definitions of the rigid body coordinate can be valid because appropriate mode functions that satisfy the geometric boundary conditions can be chosen for each case. In this paper, the rigid body mode coordinate that passes through the end-point of the beam is selected like (c) of Figure 2, and the mode functions of pin-pin boundary conditions are used to describe the displacement of the beam.

To obtain an accurate model with a small number of modes, more accurate boundary conditions were considered such as the joint hub-inertia and the end-mass in addition to the geometric pin-pin boundary condition for the mode shape functions. For the inverse dynamic model, the first two mode functions are used, and four modes are used for the manipulator model in simulation. Because of the selection of the rigid body coordinate, the end-point position of the beam can be expressed by the rigid body mode variable alone. This simple representation of the end-point position allows easy derivation of the inverse dynamics equation.

By using Lagrange's equations of motion, the dynamic equation of a flexible manipulator is obtained with generalized coordinates. The detailed derivation is given in reference [12].

$$[M]\ddot{q} + [D]\dot{q} + [K]q = [B]\tau$$

The dynamic equation can be divided into a rigid body motion part and a flexible motion part as follows:

$$\begin{bmatrix} M_{rr} & M_{rf} \\ M_{rf}^T & M_{ff} \end{bmatrix} \begin{Bmatrix} \ddot{q}_r \\ \ddot{q}_f \end{Bmatrix} + \begin{bmatrix} D_{rr} & D_{rf} \\ D_{rf}^T & D_{ff} \end{bmatrix} \begin{Bmatrix} \dot{q}_r \\ \dot{q}_f \end{Bmatrix} + \begin{bmatrix} 0 & 0 \\ 0 & K_{ff} \end{bmatrix} \begin{Bmatrix} q_r \\ q_f \end{Bmatrix} = \begin{bmatrix} B_r \\ B_f \end{bmatrix} \tau \quad (1)$$

where $q_r = q_0$: *rigid body coordinate,*

$$q_f = \begin{Bmatrix} q_1 \\ \vdots \end{Bmatrix} : \textit{flexible mode coordinate}$$

In the partitioned matrices, the subscript *r* denotes rigid; *f* denotes flexible; and the mixture, *rf*, denotes coefficients of flexible coordinates in the rigid body mode equations.

For a state space form, we obtain the following dynamic

Eq. (2). Hereafter, this dynamic equation is referred to as the direct dynamic equation to distinguish it from the inverse dynamic equation derived in Section 3.

$$\dot{X} = \begin{bmatrix} 0 & I \\ M^{-1}K & M^{-1}D \end{bmatrix} X + \begin{bmatrix} 0 \\ M^{-1}B \end{bmatrix} \tau$$

$$Y = [C]X + [F]\tau \qquad (2)$$

$$\text{where} \quad X = \{ q_r, q_f, \dot{q}_r, \dot{q}_f \}^T$$

$$= \{ q_0, q_1, \cdots, \dot{q}_0, \dot{q}_1, \cdots \}^T$$

3. Inverse Dynamic Equations

From the direct dynamic equations, the inverse dynamic equation is derived, which represents the relationship between the desired acceleration of the rigid mode (equivalent to the tip acceleration) as input and the torque as output. Equation (1) can be written in two parts:

$$[M_{rr}]\ddot{q}_r + [M_{rf}]\ddot{q}_f + [D_{rr}]\dot{q}_r + [D_{rf}]\dot{q}_f = [B_r]\tau \qquad (3)$$

$$[M_{rf}]^T\ddot{q}_r + [M_{ff}]\ddot{q}_f + [D_{rf}]^T\dot{q}_r + [D_{ff}]\dot{q}_f + [K_{ff}]q_f = [B_f]\tau \qquad (4)$$

From Eq. (3), torque is expressed as

$$\tau = [B_r]^{-1} \{ [M_{rr}]\ddot{q}_r + [M_{rf}]\ddot{q}_f + [D_{rr}]\dot{q}_r + [D_{rf}]\dot{q}_f \} \quad (3a)$$

Substitution of above Eq. (3a) into Eq. (4) gives the following relations between the flexible coordinate q_f and the rigid body coordinate q_r.

$$[M_i]\ddot{q}_f + [D_i]\dot{q}_f + [K_i]q_f = [B_{i1}]\dot{q}_r + [B_{i2}]\ddot{q}_r$$

$$\begin{aligned} \text{where} \quad [M_i] &= \{[M_{ff}] - [B_f][B_r]^{-1}[M_{rf}]\} \\ [D_i] &= \{[D_{ff}] - [B_f][B_r]^{-1}[D_{rf}]\} \\ [K_i] &= [K_{ff}] \\ [B_{i1}] &= \{[B_f][B_r]^{-1}[D_{rr}] - [D_{rf}]^T\} \\ [B_{i2}] &= \{[B_f][B_r]^{-1}[M_{rr}] - [M_{rf}]^T\} \end{aligned} \qquad (5)$$

From Eq. (4), the acceleration of the flexible coordinate is expressed as

$$\ddot{q}_f = -[M_{ff}]^{-1}[M_{rf}]^T\ddot{q}_r - [M_{ff}]^{-1}[D_{rf}]^T\dot{q}_r - [M_{ff}]^{-1}[D_{ff}]\dot{q}_f - [M_{ff}]^{-1}[K_{ff}]q_f + [M_{ff}]^{-1}[B_f]\tau \qquad (6)$$

By substituting this Eq. (6) into Eq. (3), we obtain

$$\tau = [C_{i1}]\, q_f + [C_{i2}]\, \dot{q}_f + [F_{i1}]\, \dot{q}_r + [F_{i2}]\, \ddot{q}_r \qquad (7)$$

$$\text{where} \quad [G] = \{[B_r] - [M_{rf}][M_{ff}]^{-1}[B_f]\}^{-1}$$

$$[C_{i1}] = [G]\{-[M_{rf}][M_{ff}]^{-1}[K_{ff}]\}$$

$$[C_{i2}] = [G]\{[D_{rf}] - [M_{rf}][M_{ff}]^{-1}[D_{ff}]\}$$

$$[F_{i1}] = [G]\{[D_{rr}] - [M_{rf}][M_{ff}]^{-1}[D_{rf}]^T\}$$

$$[F_{i2}] = [G]\{[M_{rr}] - [M_{rf}][M_{ff}]^{-1}[M_{rf}]^T\}$$

If Eq. (5) and Eq. (7) are represented in a state space form, the inverse dynamic equations will be written in the following simple form:

$$\text{Let} \quad X_i = \{q_f, \dot{q}_f\}^T, \quad q_{ir} = \{q_r, \dot{q}_r\}^T$$

$$\dot{X}_i = \begin{bmatrix} 0 & I \\ M_i^{-1}K_i & M_i^{-1}D_i \end{bmatrix} X_i + \begin{bmatrix} 0 & 0 \\ M_i^{-1}B_{i1} & M_i^{-1}B_{i2} \end{bmatrix} \dot{q}_{ir} \qquad (8)$$

$$\tau = [C_{i1}, C_{i2}]X_i + [F_{i1}, F_{i2}]\dot{q}_{ir}$$

$$\dot{X}_i = [A_i]X_i + [B_i]\dot{q}_{ir}$$

$$\tau = [C_i]X_i + [F_i]\dot{q}_{ir}$$

Since matrix A_i has positive real eigenvalues (which came from the positive zeros of the transfer function of the direct dynamic system) as well as negative real eigenvalues, integration of the Eq. (8) will diverge in causal sense. However, if the solution range of the equation is expanded to include noncausal solutions, a unique stable solution can be obtained by integrating this differential equation.

To analyze the inverse system of a flexible manipulator, let us define several terms. A causal system is the system in which the output (impulse response) always occurs after an input (impulse) is given. An anticausal system, on the contrary, always has the output (backward impulse response) before an input (impulse) is given. A noncausal system has the combined effect of a causal system and an anticausal

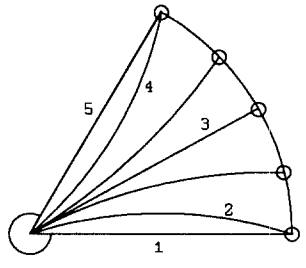

Figure 3. Point-to-point motion of a flexible manipulator

system. In order to grasp the meanings of the above definitions, the physical phenomena of the actual motion of a flexible manipulator is described using Figure 3. If a certain torque profile is applied to the manipulator, there is a unique motion of the end-point. On the other hand, if this

unique motion of the end-point is given as a desired motion, the previous torque profile should be obtained by using the inverse dynamic equations. In most cases, to make the end-point follow a certain trajectory profile, we have to preshape (prebend) the flexible manipulator like position 2 of Figure 3. Therefore, the required torque, which is necessary to preshape it, must be applied from position 1 to 2 of Figure 3 before the end-point starts to move. The torque (output of the inverse system) acts before the tip motion (input of the inverse system). This means that the inverse system has anticausal characteristics. When the flexible manipulator stops, some torque should be applied to release the flexible deflection from position 4 to 5 of Figure 3 after the end-point stops. This means that the inverse system has causal system characteristics, too. Thus, such an inverse system can be called a noncausal system, which is composed of a causal system and an anticausal system.

With this intuitive motivation, the inverse dynamic system can be divided into its causal part and its anticausal part by using the following similarity transformation:

$[T]$: *similarity transformation matrix*

$$X_i = [T]P_i$$
$$= [T_c, T_{ac}]\{P_c, P_{ac}\}^T$$

where $X_i=\{q_f, \dot{q}_f\}^T$. The T_c's basis are the eigenvectors that have negative eigenvalues, and T_{ac} is made of the eigenvectors of positive eigenvalues.

$$[T]^{-1}A_i[T] = \begin{bmatrix} A_{ic} & 0 \\ 0 & A_{iac} \end{bmatrix}$$

$$\begin{Bmatrix} \dot{P}_c \\ \dot{P}_{ac} \end{Bmatrix} = \begin{bmatrix} A_{ic} & 0 \\ 0 & A_{iac} \end{bmatrix} \begin{Bmatrix} P_c \\ P_{ac} \end{Bmatrix} + \begin{bmatrix} B_{ic} \\ B_{iac} \end{bmatrix} \dot{q}_{ir} \qquad (9)$$

$$\begin{Bmatrix} \tau_c \\ \tau_{ac} \end{Bmatrix} = \begin{bmatrix} C_{ic} \\ C_{iac} \end{bmatrix} \begin{Bmatrix} P_c \\ P_{ac} \end{Bmatrix} + \begin{bmatrix} 1/2\ F_i \\ 1/2\ F_i \end{bmatrix} \dot{q}_{ir}$$

$$\tau = \tau_c + \tau_{ac}$$

Such a coordinate change decouples the inverse system into two subsystems as shown in Eq. (9). The new variable P_c represents the coordinates of the causal system, and the P_{ac} represents the anticausal system. Even though $[F_i]$ is not required to be divided equally, it was divided equally to make the causal system and the anticausal system symmetric.

For a given end-point trajectory, the causal part of the torque is obtained by integrating the causal part of the inverse dynamic equations forward in time, starting from the initial time of the trajectory. The anticausal system equations must be integrated backward in time, starting from the final time of the trajectory. The meanings of the forward and backward integrations are interpreted in detail in frequency domain in Section 4. The total torque, which is the output of these equations, is obtained by adding the outputs of the causal and anticausal systems as shown in Figure 7.

As additional outputs, the reference trajectory of the entire flexible mode coordinates has been calculated from a rigid body mode trajectory. As can be expected from Eq. (2) and Eq. (9), the space of the full state vector X of the direct dynamic system can be divided into three subspaces: the rigid body coordinate subspace q_{ir}, the causal part flexible coordinate subspace P_c, and the anticausal part flexible coordinate subspace P_{ac}. These subspaces are linearly independent and orthogonal to each other. The relations of these spaces are illustrated in Figure 4, and is described by Eq. (10), in which only two flexible modes are considered.

$$\textit{where}\quad X=\{q_r, q_{f1}, q_{f2}, \dot{q}_r, \dot{q}_{f1}, \dot{q}_{f2}\}^T, \quad q_{ir}=\{q_r, q_t\}^T$$

$$X_i=\{q_{f1}, q_{f2}, \dot{q}_{f1}, \dot{q}_{f2}\}^T = [T]P_i$$

$$X = \begin{bmatrix} 1 & 0 \\ 0 & 0 \\ 0 & 0 \\ 0 & 1 \\ 0 & 0 \\ 0 & 0 \end{bmatrix} q_{ir} + \begin{bmatrix} 0 & 0 & 0 & 0 \\ 1 & 0 & 0 & 0 \\ 0 & 1 & 0 & 0 \\ 0 & 0 & 0 & 0 \\ 0 & 0 & 1 & 0 \\ 0 & 0 & 0 & 1 \end{bmatrix} X_i = H_r q_{ir} + H_f X_i \qquad (10)$$

$$= H_r q_{ir} + H_f[T]P_i = H_r q_{ir} + H_f T_c P_c + H_f T_{ac} P_{ac}$$

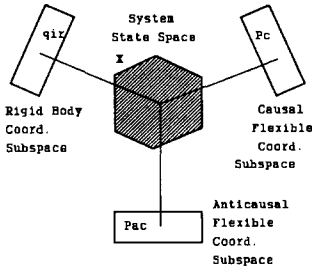

Figure 4. Dimensional analysis of state variables of flexible manipulator dynamic equations

From the given end-point trajectory, the rigid body coordinate trajectory q_{ir} is obtained. The flexible coordinate trajectories of P_c and P_{ac} are calculated from the integration of Eq. (9). Then, the trajectories of the whole states X can be obtained by using the relation given by Eq. (10). These trajectory values can be used as reference commands for feedback tracking control.

The generation of complete state trajectories is the main advantage of this time-domain inverse dynamic method over the other methods [2,3,6]. From the calculated state trajectories, the desired output trajectories can be obtained such as joint angle, joint velocity, and strains as well as the inverse dynamic torque. Because the output trajectories were obtained considering the flexible dynamics, we no longer have to give reference commands for the flexible manipulator to follow the trajectory like a rigid manipulator by letting the desired strain be zero.

4. Interpretation of the Inverse Dynamic Method in Frequency Domain

This section explains the separation of the inverse system matrix into the causal and anticausal parts by using the two-sided Laplace transform, and interprets the integration of each part equation with the convolution integral method. For simplicity, we will change the variable name $\dot{q}_{ir}$ of the

inverse dynamic equation (8) to q_a .

$$\dot{X}_i = [A_i]X_i + [B_i]q_a$$

$$\tau = [C_i]X_i + [F_i]q_a$$

Since the inverse system is noncausal ($X_i(t)$ exists for $t<0$ and $t>t_f$, when the end-point, $q_a(t)$, moves only for $0<t<t_f$), the two-sided Laplace transform should be used to obtain the transfer function of the inverse system.

The two-sided Laplace transform $L_2\{\ \}$ is defined over some strip of convergence as follows [10]:

$$X_i(s)=L_2\{X_i(t)\}$$

$$=\int_{-\infty}^{\infty} e^{-st}X_i(t)dt \qquad where \quad \alpha<Re(s)<\beta$$

Accordingly, the inverse two-sided Laplace transform is defined by

$$X_i(t)=L_2^{-1}\{X_i(s)\}$$

$$=\frac{1}{2\pi j}\int_{c-j\infty}^{c+j\infty} e^{st}X_i(s)ds \quad for \ \alpha<c<\beta$$

The strip of convergence depends on the exponential convergence rate of the time response of the function $X_i(t)$.

Define the inverse system transfer function between the input (the rigid body coordinate trajectory q_a) and the output (the joint torque τ) as

$$H(s)=\frac{\tau(s)}{q_a(s)} \qquad for \quad \alpha<Re(s)<\beta$$

Since $H(s)$ has the same order denominator and numerator, it is separated into a strictly anticausal function $H_1(s)$, a strictly causal function $H_2(s)$, and a constant K. This allows that $H_1(s)$ and $H_2(s)$ have a higher order denominator than the numerator to satisfy the condition of Jordan's Lemma [11].

$$H(s) = H_1(s) + H_2(s) + K \qquad (11)$$

Since the impulse response $h(t)$ depends on the choice of the strip of convergence, the shaded region of Figure 5 between the largest negative pole, $a1$, and the smallest positive pole, $b1$, has been chosen among several candidate strips of convergence such as $Re(s)<a2$, $a2<Re(s)<a1$, $a1<Re(s)<b1$, ... Among them, only the shaded region

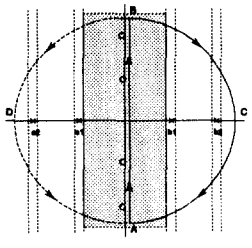

Figure 5. Contour integrals in complex plane

provides a bounded stable time response for the inverse Laplace transform. Because the particular strip of convergence is chosen, $H(s)$ is seperated to $H_1(s)$ that has only positive poles corresponding to the eigenvalues of anticausal part system matrix A_{ac}, and $H_2(s)$ that has only negative poles corresponding to the eigenvalues of the causal part system matrix A_c. These explanations justify why the inverse system matrix A_i can be separated into A_{ac} having only positive eigenvalues, and A_c having only negative eigenvalues, by using the particular transformation matrix $[T_{ac}, T_c]$.

The inverse Laplace transform of Eq. (11) is calculated along line AB in the strip of $a1< Re(s)<b1$ [10]. Using the theorem on integration over large semicircles and Jordan's Lemma [11], the above complex-plane contour integral along line AB of Figure 5 is calculated as follows:

$$\begin{aligned} for\ t<0 \quad h(t) &= \frac{1}{2\pi j}\oint_{ABCA} e^{st}H(s)ds \\ &= \frac{1}{2\pi j}\int_{c-j\infty}^{c+j\infty} e^{st}H_1(s)ds + \delta(t)\,K \\ &= \sum residue\ of\ e^{st}H_1(s) + \delta(t)\,K \\ &= h_{ac}(t) + \delta(t)\,K \end{aligned} \qquad (12)$$

$$\begin{aligned} for\ t>0 \quad h(t) &= \frac{1}{2\pi j}\oint_{ABDA} e^{st}H(s)ds \\ &= \frac{1}{2\pi j}\int_{c-j\infty}^{c+j\infty} e^{st}H_2(s)ds + \delta(t)\,K \\ &= \sum residue\ of\ e^{st}H_2(s) + \delta(t)\,K \\ &= h_c(t) + \delta(t)\,K \end{aligned} \qquad (13)$$

The inverse Laplace transform of Eq. (12) and Eq. (13) gives the impulse response function $h(t)$ which has an anticausal part, $h_{ac}(t)$, and a causal part, $h_c(t)$.

Next, the total torque calculation adding the causal part of the torque and the anticausal part of the torque will be interpreted with the convolution integral.

$$\tau(t) = L_2^{-1}\{H(s)q_a(s)\}$$

$$= \int_{-\infty}^{\infty} h(\eta)\ q_a(t-\eta)d\eta$$

where $q_a(t)$ *is defined for* $0\le t\le t_f$, *and* 0 *otherwise.*

Since $h(t)=h_{ac}(t)+\delta(t)K$ *for* $t\le 0$, $h_{ac}(t)=0$ *for* $t>0$,

and $h(t)=h_c(t)+\delta(t)K$ *for* $t\ge 0$, $h_c(t)=0$ *for* $t<0$,

$$\begin{aligned} \tau(t) &= \int_{-\infty}^{0} h_{ac}(\eta)q_a(t-\eta)d\eta + \int_{0}^{\infty} h_c(\eta)q_a(t-\eta)d\eta \\ &\quad + \int_{-\infty}^{\infty} \delta(\eta)Kq_a(t-\eta)d\eta \\ &= \tau_{ac}^{*}(t\le t_f) + \tau_c^{*}(t\ge 0) + K\ q_a(0\le t\le t_f) \\ &= \{\tau_{ac}^{*}(t) + \frac{1}{2}K\ q_a(t)\} + \{\tau_c^{*}(t) + \frac{1}{2}K\ q_a(t)\} \\ &= \tau_{ac} + \tau_c \end{aligned} \qquad (14)$$

where $\tau_{ac}^{*}=0$ $t>t_f$, $\tau_{ac}^{*}=0$ $t<0$, $q_a=0$ $t<0$ *and* $t>t_f$

The torque Eq. (14) has the same form as Eq. (9). The first convolution integral of τ_{ac}^{*} is equivalent to the backward integration of the anticausal part system equation from t_f to $-\infty$; the second integral is the same as the integration of the causal part equation from 0 to ∞. Thus, the total torque is composed of the anticausal part torque τ_{ac}^{*}, the causal part torque τ_c^{*}, and the input feedforward term Kq_a, which coincides with the term $[F_l]q_a$ of the inverse dynamic equation.

5. Trajectory Generation

Theoretically, the inverse dynamic equation can give a torque profile for an arbitrary acceleration profile. However, as Bayo mentioned in reference [3], it is important to apply an acceleration profile that does not excite the unmodeled dynamics of a manipulator. If the acceleration changes sharply, the calculated torque profile may excite the unmodeled high frequency modes of the flexible manipulator. Furthermore, the torque frequency may be beyond the actuator bandwidth. In addition to the above constraint, the maximum acceleration limit should be chosen properly to avoid saturation of the actuator and to use its full capacity for minimum traveling time. This constraint makes the acceleration profile close to a bang-bang type, which will result in unwanted high frequency problems. Therefore, the acceleration profile has to be selected by compromising the profile smoothness and the use of the full actuator capacity within its limit.

Considering the above constraints, the acceleration profile of Figure 6 was suggested. It is composed of four third-order polynomial parts and two constant acceleration parts. The

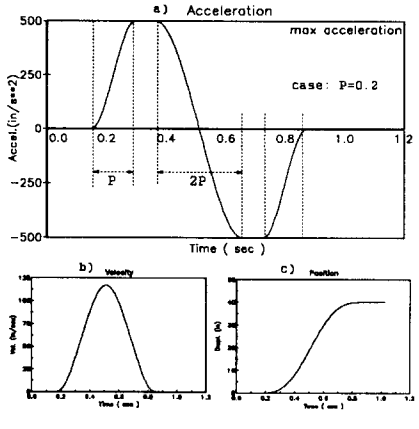

Figure 6. Desired end point trajectory: (a) acceleration, (b) velocity, (c) position

parameter P is the ratio of the first part polynomial acceleration time to the total end-point traveling time. If P=0, the profile will be the bang-bang type. And, if P=0.25, the profile will be very smooth by being connected with four polynomials without constant acceleration parts. For simulations and experiments, the P=0.2 case was used.

6. Simulation Results of the Inverse Dynamic Control

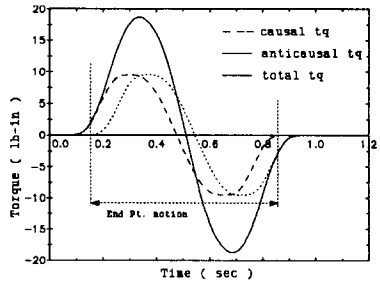

Figure 7. Calculation of torque with the inverse dynamic method

This section presents simulation results to illustrate the performance of the inverse dynamic method. First, the total torque profile is calculated from the causal part and the anticausal part of Eq. (9) for a given end-point acceleration profile, as shown in Figure 7. The desired trajectories of the output such as joint angle, joint velocity, and strains are generated and are shown in Figure 8.

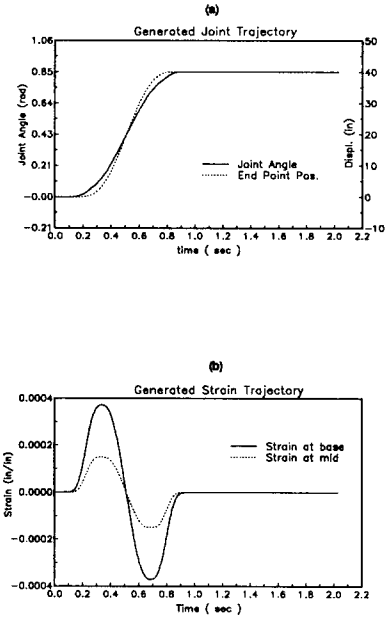

Figure 8. Trajectory generation by using the inverse dynamic method: (a) joint angle, (b) strain at base, and at midpoint

Second, the calculated torque was applied to the ideal flexible manipulator model from which the inverse dynamic model was derived. As shown in Figure 9, the end-point follows the desired trajectory exactly; and no undershoot, overshoot, or noticeable residual vibration occurs. However, the strain plot shows some residual oscillations after the end-point stops. These oscillations are due to numerical integration errors that results from the somewhat slow

sampling frequency (150 Hz) used in the simulation, which is the same as the sampling frequency of the experiment. When much higher sampling frequency was used, the residual vibration was almost unnoticeable.

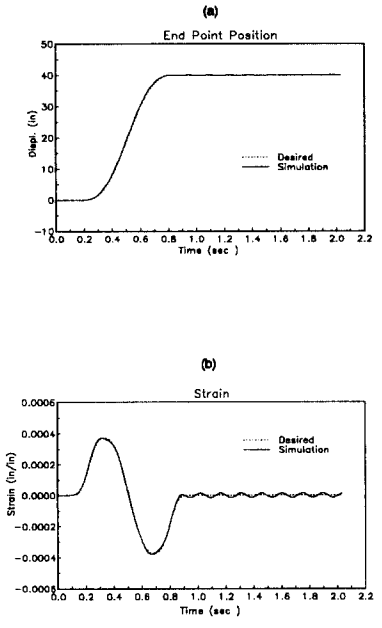

Figure 9. Simulation of the open-loop control with the inverse dynamic method: (a) end-point position, (b) strain at base

Next, the effectiveness of inverse dynamic trajectories, which considered flexible dynamics, is demonstrated by comparing the simulation results of several typical feedback control methods. Figure 10 (curve a) is the result of a collocated joint PD controller for a step input command. As can be expected, the feedback of position error generates very high peak torque at the beginning, and it excites the system natural frequencies. Therefore, it requires relatively long settling time. The result also shows the undershoot and the overshoot of the end-point position.

As an alternative method, a tracking full-state feedback controller was tried with a nominal joint trajectory. The nominal joint trajectory means that the trajectory is generated from the relation $\theta = X_e / L$ between the joint and the end-point position based on rigid-link assumption. Consequently, the desired flexible coordinate values were set to zero, $q_f = 0$, $\dot{q}_f = 0$. The feedback gain was selected by the LQ method. Even though the response (curve b) is better than that of the step input joint feedback case, it still has overshoot and requires a relatively long settling time. This poor tracking response is due to the unnatural commands that assign zero values to the flexible coordinate commands without considering flexible dynamics. If a more natural reference commands of flexible modes are used, which was obtained from the inverse dynamic method, we can obtain good tracking performance. Figure 10 (curve c) shows almost no tracking errors, no overshoot, and no vibration. This comparison clearly demonstrates the advantage of complete state trajectory generation by using the inverse dynamic method.

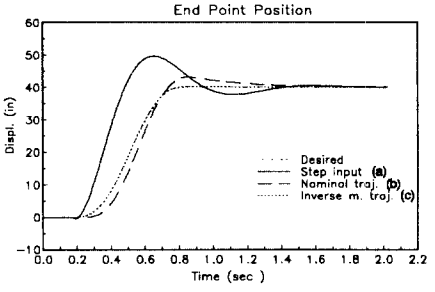

Figure 10. Comparison of typical trajectories for feedback control methods: a) step input for joint feedback, b) nominal trajectory for full state feedback, c) inverse dynamic trajectory for full state feedback

7. Experimental Results

Although the open-loop control with the inverse dynamic method showed the good simulation results with an ideal model in Figure 9, it produced a large positioning error with the experimental manipulator due to the effects of the joint friction. Therefore, a tracking controller was designed with the feedforward inverse dynamic control as shown in Fig. 11. A joint feedback control loop was added to provide robustness to the system, and a friction compensation loop was also added to cancel the effect of the friction force.

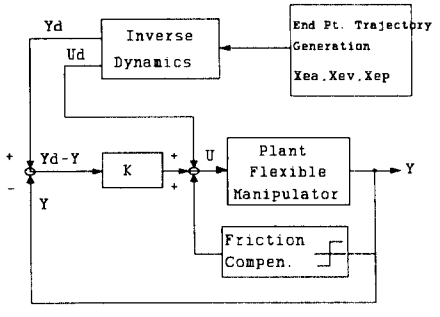

Figure 11. Tracking control scheme of the experiment

The combined tracking control scheme of the inverse dynamic feedforward control and the feedback control was implemented to the single-link flexible manipulator. The manipulator used in the experiment has a 47-in.-long arm and a 0.1 LB end mass. It is driven by an Inland D.C. servo motor with a current amplifier. For a real-time control, a Micro Vax II was used with 12-bit A/D and D/A boards. The off line calculation of the trajectory and the torque profile was also performed by using the Micro Vax.

By applying the precalculated torque, compensating the joint friction, and using the feedback of the tracking error at

the joint, the excellent results of Figure 12 were obtained. The flexible manipulator could stop without any overshoot or any residual vibration after it moved 40 in. (48.76 degrees) within less than 0.8 s. In the strain signal, rough jerk exists that could be eliminated by using a smoother acceleration profile. Unfortunately, since the end-point position sensor was not available, the end-point position could not be measured directly. However, the end-point tracking performance can be estimated from the joint tracking and the strain tracking result. If the joint does not have any overshoot or vibration and the strain does not show any residual vibration, the end-point can be presumed to stop without any overshoot or vibration.

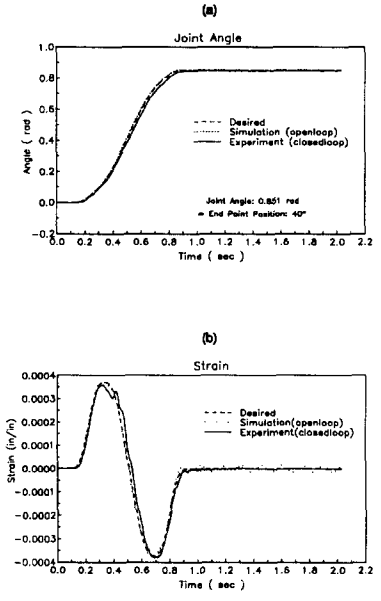

Figure 12. Experimental results of the tracking control combined with the inverse dynamic feedforward control and the joint feedback control: a) joint angle, b) strain at the base

In the experiment, only joint angle and joint velocity signals were used for feedback. The experimental results show that a simple joint feedback PD controller performs excellent tracking, if it is combined with the inverse dynamic feedforward control, and if the joint trajectories are provided considering the flexible dynamics.

8. Conclusion

The proposed inverse dynamic method provides a simple way to generate the required torque profile and entire state trajectories in the time domain for a flexible manipulator. The use of the generated flexible coordinate trajectories showed much better feedback tracking performance than the case of nominal trajectory commands based on rigid-link assumption in simulation. In laboratory experiments, the feedforward control using the inverse dynamic method showed good tracking performance with a simple joint feedback controller. It was observed that the measured outputs showed very small tracking error, no overshoot, and no oscillation; and they agree well with the simulation results.

The characteristics of the inverse dynamic system of a flexible manipulator were newly interpreted with the use of causal and anticausal concepts. Based on these concepts, the time-domain inverse dynamic method was interpreted in frequency domain in detail by using the two-sided Laplace transform in the frequency domain and the convolution integral.

Although several successful results of this method are mentioned, this inverse dynamic method is limited to linear systems. In order to be extended for a multilink flexible manipulator, this method should be incorporated with a nonlinear inversion technique, or the dynamics of the manipulator should be linearized along the desired end-point trajectory.

References

1. Asada, H. and Ma, Z., "Inverse Dynamics of Flexible Robots," *Proceedings of the American Control Conference*, pp. 2352-2359, 1989.

2. Bayo, E., "A Finite Element Approach to Control the End-Point Motion of a Single-Link Flexible Robot," *Journal of Robotic Systems*, Vol. 4, No. 1, pp. 63-75, 1987.

3. Bayo, E. and Paden, B., "On Trajectory generation for Flexible Robots," *Journal of Robotic Systems*, Vol. 4, No. 2, pp. 229-235, 1987.

4. Bayo, E. and Moulin, H., "An Efficient Computation of the Inverse Dynamics of Flexible Manipulators in the Time Domain," *Proceedings of IEEE Conference on Robotics and Automation*, pp. 710-715, 1989.

5. Cannon, R. and Schmitz, E., "Initial Experiments on End-point Control of a Flexible One-Link Robot," *International Journal of Robotics Research*, Vol. 3, No. 3, pp. 49-54, 1984.

6. De Luca, A. and Siciliano, B., "Joint-Based Control of a Nonlinear Model of a Flexible Arm," *Proceedings of the American Control Conference*, pp. 935-940, Atlanta, June 1988.

7. Hastings, G. and Book, W. J., "Experiments in the Optimal Control of A Flexible Manipulator," *Proceedings of the American Control Conference*, pp.728-729, Boston, 1985.

8. Oosting, K. and Dickerson, S. L., "Simulation of a High-Speed Lightweight Arm," *Proc. of IEEE International Conference on Robotics and Automation*, pp. 494-496, Philadelphia, 1988.

9. Wang, D. and Vidyasagar, M., "Modelling and Control of Flexible Beam Using the Stable Factorization Approach," *Proceedings of ASME Winter Annual Meeting, Robotics: Theory and Application*, Dec. 1986.

10. Pol, Balth. V. D. and Bremmer, H., *Operational Calculus Based on the Two-Sided Laplace Transform*, University Press at Cambridge, 1955

11. LePage, Wilbur R., *Complex Variables and the Laplace Transform for Engineers*, McGraw-Hill Book Co., 1961

12. Kwon, D.-S. and Book, W. J., "An Inverse Dynamic Method Yielding Flexible Manipulator State Trajectories," *Proceedings of the American Control Conference*, Vol. 1, pp. 186-193, San Diego, May 1990.